Modelling low-energy electron–molecule capture processes†

E. I. Dashevskaya,[bc] I. Litvin,[bc] E. E. Nikitin[bc] and J. Troe*[ab]

Received 11th September 2007, Accepted 19th November 2007
First published as an Advance Article on the web 6th December 2007
DOI: 10.1039/b713530k

Cross sections and rate coefficients for capture of low-energy electrons with polar and polarizable target molecules are calculated in the framework of Fabrikant and Hotop's extended version of the Vogt–Wannier model and an extension of this approach is given in the present article. Analytical approximations are derived in order to facilitate the application to experiments. A comparison with a selection of experimental electron attachment rate coefficients provides insight into the competition between anion formation through electron capture and scattering processes which do not follow this pathway.

1. Introduction

The dynamics of low-energy electron–molecule collisions can be understood in the framework of a variety of scattering models. Hotop, Ruf, Allan, and Fabrikant[1] have presented a detailed state-of-the-art review. There is a multichannel R-matrix theory which focuses on resonance phenomena caused by the interaction of incoming and outgoing wavepackets. Considering incoming waves only, there is also an electron–molecule capture theory such as formulated by Vogt and Wannier[2] and extended by Fabrikant and Hotop.[3] This approach appears to be suitable when anions are formed and the outgoing wavepacket is attenuated by intramolecular vibrational redistribution (IVR) of the nuclear framework. The electron–molecule capture concept finds its equivalence in capture theory for atom–molecule (neutral or charged) collisions and it leads over to the analysis of the kinetics of barrierless processes in reaction kinetics.[4] The combination of capture theory with statistical theories of the dynamics of adducts then allows one to cope with a variety of more complex kinetic phenomena that are initiated by the capture process. One would expect that such phenomena for electron–molecule capture can then be described in a similar way as in neutral gas phase kinetics.

The present article aims at simple representations of an electron–molecule capture, suitable to be combined with the statistical unimolecular rate theory applied to metastable anionic states. We intend to cast the Vogt–Wannier, extended Vogt–Wannier, and related treatments into the simplest possible analytical form such that electron–molecule "collision numbers" can be defined and an application to experiments can be readily made. A simple approximation for polarizable target molecules and s-wave scattering has already been proposed by Klots[5] and is widely used by experimentalists. It was shown in ref. 1, however, that the Klots s-wave capture cross section differs from the accurate numerical Vogt–Wannier result by up to about 8%. In our present work we first modify the Klots expression in a very simple way which allows us to reduce the error by about one order of magnitude. In addition, we provide analytical approximations for higher partial-wave capture cross sections with polarizable target molecules up to $l = 4$. We then inspect expressions for electron capture cross sections for polar plus polarizable target molecules, following and further elaborating Fabrikant and Hotop's[3] extended Vogt–Wannier model. We focus our attention on s-wave scattering, elaborate capture cross sections, and provide analytical approximations to capture rate coefficients. We finally also consider all-wave capture and compare quantum with classical trajectory results.

Having in hand simple expressions for electron–molecule capture cross sections and rate coefficients, one can systematically compare the calculations with experimental electron attachment data. In selected cases one finds close agreement. In the majority of experiments, however, the capture theory overestimates attachment rates and cross sections. In this case, elastic and inelastic (or also direct dissociative) electron scattering effectively competes with IVR-induced anion formation. In practice, one would certainly like to rationalize the partitioning of electron–molecule collisions between attachment and (in)elastic scattering channels, but this is a more difficult task which will be the aim of a later analysis.[6] One system, where attachment at low electron energies is dominated by capture, is the nondissociative and dissociative electron attachment to SF_6. It was shown in ref. 7 and 8 that the combination of the Vogt–Wannier capture and the statistical unimolecular rate theory (with some empirical modifications accounting for the contribution from IVR and direct vibrational excitation) can enable modelling of many kinetic observables. In other systems, attachment rates are markedly, sometimes orders of magnitude, smaller than those given by the capture theory. For these cases, a simple capture theory such as that presented in this work at least provides an upper bound and gives an orientation for the competition between anion formation and direct scattering processes.

[a] *Institut für Physikalische Chemie, Universität Göttingen, Tammannstr. 6, D-37077 Göttingen, Germany. E-mail: shoff@gwdg.de*
[b] *Max-Planck-Institut für biophysikalische Chemie, Am Fassberg 11, D-37077 Göttingen, Germany*
[c] *Schulich Faculty of Chemistry, Technion-Israel Institute of Technology, Haifa, 32000, Israel*

† The HTML version of this article has been enhanced with colour images.

It should be emphasized that capture theories of the present type assume complete incorporation of the incoming electron into the electronic cloud of the target molecule and do not account for outgoing wavepackets. Neither resonance phenomena caused by interaction of incoming and outgoing wavepackets, nor inelastic scattering processes without formation of anionic states, are thus represented by this approach. Nevertheless, upper bound calculations of cross sections for capture appear always useful to be made. For further discussions of the relation between resonance and capture theories, see ref. 1.

2. Electron capture by polarizable target molecules

In the present article we follow the treatment of ref. 4. Capture cross sections $\sigma(E)$ are calculated by solving a 1-D Schrödinger equation with standard scattering boundary conditions at large electron–molecule separations R and with an incoming wave only at small values of R near the complex boundary. For a spherically symmetric interaction such as for the polarization potential, $\sigma(E)$ is represented by

$$\sigma(k) = (\pi/k^2)\sum_{l=0}^{\infty}(2l+1)P_l(k) \qquad (2.1)$$

with the wave vector $k = p/\hbar$ of the relative motion, $E = p^2/2\mu$, and the probability $P_l(k)$ for l-wave capture. Using dimensionless reduced wave vectors κ given by

$$\kappa = k(\mu e^2\alpha)^{1/2}/\hbar = \mu e(2\alpha E)^{1/2}/\hbar^2 \qquad (2.2)$$

with the reduced mass μ, the electronic charge e, and the polarizability α of the molecular target, the capture probabilities are expressed as $P_l(\kappa)$. A simple analytical fit to s-wave capture probabilities ($l = 0$) in the form of

$$P_s(\kappa) = P_{l=0}(\kappa) \approx 1 - \exp(-4\kappa) \qquad (2.3)$$

was proposed by Klots[5] some time ago and for convenience was often used in practical applications. It leads to the correct low-energy limit $P_{l=0}(\kappa) \to 4\kappa$ for $\kappa \to 0$. Likewise, it goes to the correct high-energy limit $P_s(\kappa) \to 1$ for $\kappa \gg 1$. However, it was shown in ref. 1 that the Klots expression at values near $\kappa = 1$ deviates from the accurate results, obtained by numerically solving the Schrödinger equation, up to about 8%. Inspecting numerical solutions again, we found that a simple modification of Klots' equation considerably improves the accuracy. The expression

$$P_s(\kappa) = P_{l=0}(\kappa) \approx 1 - 0.5\exp(-2\kappa) - 0.5\exp(-6\kappa) \quad (2.4)$$

was found to be about a factor of 5 more precise than the Klots expression. Modifying this expression slightly more by putting

$$P_s(\kappa) \approx 1 - 0.25\exp(-1.387\kappa) - 0.75\exp(-4.871\kappa) \quad (2.5)$$

improves the accuracy of the Klots expression by about one order of magnitude. The results of eqns (2.3)–(2.5) in Fig. 1 are compared with accurate numerical results. Eqn (2.5) nowhere differs from the accurate results by more than 0.8% and thus supersedes Klots' eqn (2.3). (Low amplitude undulations at very small values of κ are due to errors in the numerical integration of the capture equations. They practically do not affect the calculations of temperature-dependent rate coefficients.)

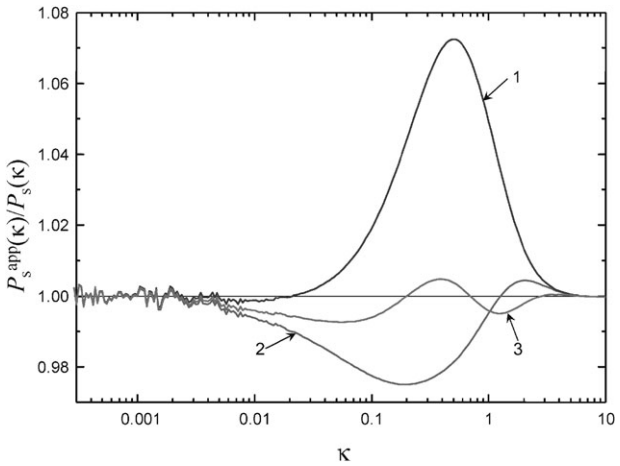

Fig. 1 Comparison of analytical approximations for the s-wave capture probabilities $P_s^{app}(\kappa)$ with numerically accurate s-wave capture probabilities $P_s(\kappa)$ for dipole-less polarizable target molecules (curve 1: Klots approximation from eqn (2.3), curve 2: double-exponential approximation from eqn (2.4), curve 3: double-exponential approximation from eqn (2.5)).

Capture by molecular targets with low to medium polarizabilities is generally assumed to be governed by s-waves. Higher values of l appear to be relevant only for objects with large polarizabilities.[1] For completeness, we also calculated $P_l(\kappa)$ for $l = 1, 2, 3$, and 4 and again represented the results in approximate analytical form. The Appendix provides the corresponding equations.

Thermal averaging of the capture cross sections leads to capture of rate coefficients which is easily done with the analytical approximation for s-waves given in eqns (2.3)–(2.5). Following again the treatment of ref. 4, the capture rate coefficients $k_{cap}(T)$ are expressed in a dimensionless reduced form through

$$\chi(T) = k_{cap}(T)/k_L \qquad (2.6)$$

where k_L denotes the Langevin rate constant

$$k_L = 2\pi e(\alpha/\mu)^{1/2} \qquad (2.7)$$

Employing a reduced temperature θ

$$\theta = (e\mu/\hbar^2)^2\alpha kT \qquad (2.8)$$

and a thermal distribution $F(\kappa, \theta)$

$$F(\kappa,\theta) = (2\pi\theta)^{-1/2}(2\kappa^2\theta^{-1})\exp(-\kappa^2/2\theta) \qquad (2.9)$$

partial-wave and all-wave rate coefficients are easily obtained. For instance, dimensionless s-wave rate coefficients are calculated from

$$\chi_s(\theta) = \int_0^{\infty}(2\kappa)^{-1}P_s(\kappa)F(\kappa,\theta)\mathrm{d}\kappa \qquad (2.10)$$

and all-wave rate coefficients follow as

$$\chi_{\mathrm{all}}(\theta) = \sum_{l=0}^{\infty} (2l+1) \int_0^{\infty} (2\kappa)^{-1} P_l(\kappa) F(\kappa, \theta) \mathrm{d}\kappa \qquad (2.11)$$

The low- and high-temperature limits of $\chi_s(\theta)$ are easily found to be

$$\chi_s(\theta \to 0) = 2 \qquad (2.12)$$

which is called the Bethe–Wigner limit, and

$$\chi_s(\theta \to \infty) = (2\pi\theta)^{-1/2} \qquad (2.13)$$

which is a decreasing function of θ in contrast to the temperature-independent all-wave Langevin limit $\chi_{\mathrm{all}}(\theta \to \infty) = 1$. Employing $P_s(\kappa)$ from eqn (2.3)–(2.5), $\chi_s(\theta)$ at intermediate values of θ can also be evaluated in analytical form. *E.g.*, with eqn (2.5) one obtains

$$\chi_s(\theta) \approx 0.173 \exp(0.962\theta)\{1 - \mathrm{erf}[(0.962\theta)^{1/2}]\} + 1.827 \exp(11.863\theta)\{1 - \mathrm{erf}[(11.863\theta)^{1/2}]\} \qquad (2.14)$$

where the error function is given by $\mathrm{erf}(x) = (2/\pi^{1/2}) \int_0^x \exp(-t^2)\mathrm{d}t$.

Partial-wave capture rate coefficients in principle could also be expressed in analytical form with the expressions for cross sections given in Appendix A1. However, numerical calculations are more appropriate, which also applies to the all-wave capture rate coefficient $\chi_{\mathrm{all}}(\theta)$. For the latter we have done this calculation and plotted the result in ref. 4, see also section 3. For convenience, in the present work, we have derived an analytical approximation to the all-wave rate coefficient $\chi_{\mathrm{all}}(T)$ which is given by

$$\chi_{\mathrm{all}}(\theta) \approx 1.5 - 0.5 \tanh(0.925\xi + 1.08\xi^2 + 0.04\xi^3) \qquad (2.15)$$

with $\xi = 2.075 + \log_{10}(\theta)$. The low- and high-temperature limits of $\chi_{\mathrm{all}}(\theta)$ now are $\chi_{\mathrm{all}}(\theta \to 0) = \chi_s(\theta \to 0) = 2$ and $\chi_{\mathrm{all}}(\theta \to \infty) = 1$ where the latter corresponds to the classical limit given by the Langevin rate constant. We do not plot the derived expressions for cross sections or rate coefficients at this stage, because they will be illustrated as zero-dipole moment limits of the treatment of the next section.

3. s-Wave electron capture by polar plus polarizable target molecules

When the polarizable target molecule also has a permanent dipole moment μ_D, the electron–molecule interaction potential is anisotropic and approximately of cos γ-form (with γ being the angle between the dipole axis and the line connecting the position of the electron with the molecular center of mass). In the sudden limit of the dynamics, which applies to the electron capture considered here, the orientation of the molecular target can be assumed to be fixed in space. The radial Schrödinger equation, instead of γ, will then contain a parameter $\tilde{D}$ and have the form[1]

$$\left\{ -\frac{\hbar^2}{2\mu}\frac{\partial^2}{\partial R^2} + \frac{\hbar^2 \tilde{D}}{2\mu R^2} - \frac{e^2\alpha}{2R^4} \right\} \varphi = E\varphi \qquad (3.1)$$

where $\tilde{D}$ represents the eigenvalues of the operator $\hat{D} = \hat{\boldsymbol{l}}^2 - 2d \cos\gamma$ with the angular momentum operator $\hat{\boldsymbol{l}}^2$ and the parameter $d = e\mu\mu_D/\hbar^2$. Interestingly, the eigenvalues of the matrix D, which are needed for the formulation of the capture eqn (3.1), in the sudden limit, formally coincide with the eigenvalues of a rigid dipolar rotor in a uniform electrical field such as evaluated in Stark spectroscopy, see ref. 9–13 for analytical approximations. These eigenvalues can be expressed by D_{jm} where j and m are free rotor quantum numbers.

The solution of eqn (3.1) with $\tilde{D} = D_{jm}$, by analogy to the treatment of ref. 4 such as that also employed in section 2, leads to the capture probabilities $P_{jm}(\kappa)$ to be used in an expression similar to eqn (2.1). However, in what follows we only consider the lowest eigenvalue D_{00} from the set $\tilde{D}$ which we call D_s in order to draw attention to the analogy with s-wave capture. This corresponds to the "extended Vogt–Wannier model" such as that elaborated by Fabrikant and Hotop.[1,3]

As in ref. 4 and section 2, we express eqn (3.1) again in dimensionless variables with $R_L = e(\mu\alpha)^{1/2}/\hbar$, $\rho = R/R_L$, $\kappa = kR_L$, and $\varepsilon = \kappa^2/2 = (\mu R_L^2)E$, such that, for the lowest eigenvalue D_s, the capture eqn (3.1) writes

$$\left\{ -\frac{\partial^2}{2\partial\rho^2} + \frac{D_s}{2\rho^2} - \frac{1}{2\rho^4} \right\} \varphi_\varepsilon(\rho, D_s) = \varepsilon\varphi_\varepsilon(\rho, D_s) \qquad (3.2)$$

The eigenvalues D_s for small values of the parameter d can be readily found within second-order perturbation approximation. One obtains, *e.g.*,

$$D_s \approx -(2/3)d^2 \qquad (3.3)$$

Beyond second order and with d not exceeding a critical value of 0.639 (corresponding to $\mu_D \approx 1.625$ Debye), an approximation of the form,[1]

$$D_s \approx \lambda(1+\lambda) \qquad (3.4)$$

with

$$\lambda = -0.5 + 0.5[1 - 4d^2(0.666 - 0.156d^2 + 0.050d^4)]^{1/2} \qquad (3.5)$$

has been recommended in ref. 1 and 3. Higher perturbation results as well as perturbation results for small values of d^{-1} and analytical interpolations between the ranges of small d and small d^{-1} are also available, see ref. 9–13. Fig. 2 compares accurate numerical results for $D_s(d)$ with the parabolic approximation of eqn (3.3) and the approximation of eqns (3.4) and (3.5).

Employing the described eigenvalues D_s in eqn (3.2), the radial Schrödinger equation is solved and leads to the capture probabilities. *E.g.*, on the basis of eqns (3.4) and (3.5), over the range $-1/4 < D_s \leq 0$ and for $\kappa \ll 1$, Fabrikant and Hotop[3] recommended

$$P_s(\kappa, D_s) \approx 4 \sin^2(\pi\tau)/[b^2 + b^{-2} - 2\cos(2\pi\tau)] \qquad (3.6)$$

with $\tau = (D_s + \frac{1}{4})^{1/2}$ and

$$b = (\kappa/4)^{\tau} \Gamma(1-\tau)\Gamma(1+\tau) \qquad (3.7)$$

In order to verify the accuracy of eqns (3.6)–(3.7), we have numerically solved eqn (3.2) and plotted the results in Fig. 3.

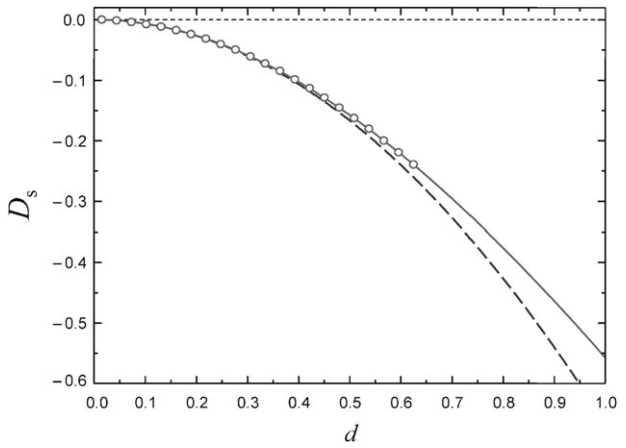

Fig. 2 Dependence of the s-wave eigenvalue D_s on the reduced dipole moment $d = e\mu\mu_D/\hbar^2$ of a polar target (full line: numerical results, dashed line: parabolic approximation from eqn (3.3), circles: analytical approximation from eqns (3.4) and (3.5)).

In these calculations we have extended the range of D_s down to values below $-1/4$. Our results are consistent with the prediction that the limit of $P_s(\kappa, D_s)$ for $D_s > -1/4$ and $\kappa \to 0$ is zero, while for $D_s \leq -1/4$ it assumes a non-zero value. For $D_s = 0$, *i.e.* for $\tau = 1/2$ in eqn (3.6), the correct low-energy capture probability for a polarizable target with $\mu_D = 0$ is obtained, *i.e.* $P_s(\kappa) \to 4\kappa$ such as that given by eqns (2.3)–(2.5).We can also see that the numerical results begin to deviate noticeably from eqn (3.6) at κ above about 0.2 which is somewhat lower than suggested in ref. 3. Passing from $P_s(\kappa, D_s)$ to $P_s(\kappa, d)$, one obtains Fig. 4. Again one can see up to which values of κ the analytical solutions by Fabrikant and Hotop[3] provide good results. One can also notice that $P_s(\kappa)$ approaches unity when d exceeds unity. Inserting $P_s(\kappa)$ into eqn (2.10) gives χ_s, see Fig. 5.

The following properties of $\chi_s(\theta, d)$ are worth mentioning: (i) The lower limit of $\chi_s(\theta, d)$ corresponds to $P_s(\kappa, \theta)$ for $\mu_D = 0$ ($d = 0$), *i.e.* to $\chi_s(\theta)$ from section 2. It is described by the analytical approximation in eqn (2.14) and represented by the filled circles. (ii) The upper limit of $\chi_s(\theta, d)$ corresponds to $P_s(\kappa, \theta) = 1$. It is given by the analytical expression $\chi_s^{max}(\theta) = 1/\sqrt{2\pi\theta}$ and represented by the dashed line in Fig. 5. Note that $\chi_s^{max}(\theta) = 1/\sqrt{2\pi\theta}$ is not much higher than $\chi_s(\theta, d)$ for $d = 1$. (iii) The low-temperature limit of $\chi_s(\theta, d)$, *i.e.* $\chi_s(\theta, d)|_{\theta \ll 1}$, which is derived from the analytical formulae (3.6) and (3.7), reads

$$\chi_s(\theta, d)|_{\theta \ll 1} = (\theta/8)^{\tau - 1/2} \frac{\sin^2(\pi\tau)}{\sqrt{\pi}} \times \frac{\Gamma^2(1-\tau)}{\Gamma(1+\tau)} [1 + O((\theta/8)^{\tau})] \quad (3.8)$$

where $O(x)$ means of the order of x. Note that the correction term $O(x)$ in the bracket of eqn (3.8) for small θ is small as long as τ is not too small. This peculiarity of the expansion of $\chi_s(\theta, d)$ in powers of θ reflects a similar behaviour of $P_s(\kappa, d)$ in an expansion in powers of κ (see the comments in ref. 3 that follow eqn (20)). (iv) Under general conditions, one may either use the graphical representation of $\chi_s(\theta, d)$ in Fig. 5 or employ

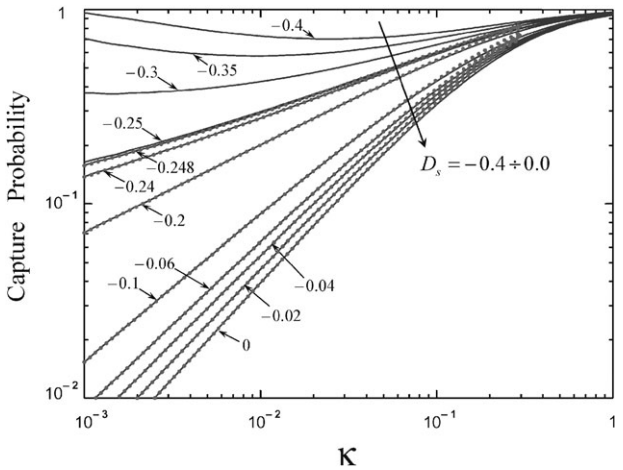

Fig. 3 Capture probabilities $P_s(\kappa, D_s)$ for subcritical ($-0.25 < D_s \leq 0$) and supercritical ($D_s \leq -0.25$) values of the "effective s-wave" eigenvalue D_s (full lines: numerical results, dots: analytical Fabrikant–Hotop approximation from eqns (3.6) and (3.7) truncated at $\kappa = 0.3$).

the following approximate relationship which expresses $\chi_s(\theta, d)$ between $\chi_s(\theta)$ (introduced in section 2) and the quantity $\chi_s^{max}(\theta)$, (defined above)

$$\chi_s(\theta, d) \approx \chi_s(\theta) + [\chi_s^{max}(\theta) - \chi_s(\theta)] \times \{1 - \exp[-G(\theta, d)]\} \quad (3.9)$$

where $G(\theta, d)$ denotes

$$G(\theta, d) = [1.55 + 0.289 \log_{10}(\theta)](d^{2.2} + d^{4.2}) \quad (3.10)$$

Eqns (3.9) and (3.10) approximate the accurate numerical results illustrated in Fig. 5 within better than 5% as long as $\chi_s(\theta, d)$ does not exceed a value of 4.

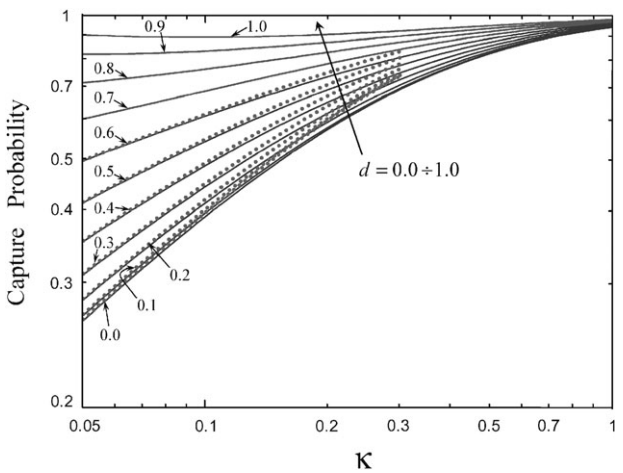

Fig. 4 Capture probabilities $P_s(\kappa, d)$ for different values of the reduced dipole moments d, full lines: numerical results, dots: analytical Fabrikant–Hotop approximation from eqns (3.6) and (3.7) truncated at $\kappa = 0.3$).

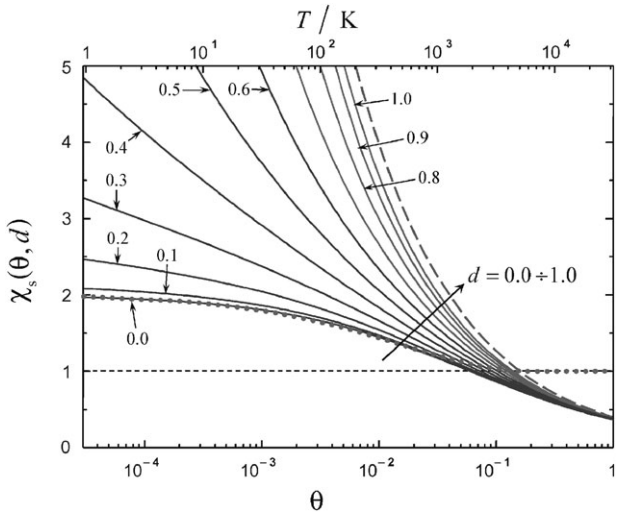

Fig. 5 Accurate reduced thermal s-wave capture rate coefficients $\chi_s(\theta, d)$ as a function of the reduced temperature θ eqn (2.8) and for different reduced dipole moments $d = e\mu\mu_D/\hbar^2$ (full lines: numerical results, dots: all-wave capture for $d = 0$ from ref. 4, the temperature scale on the upper abscissa is for a representative polarizability of $\alpha = 1.48 \times 10^{-24}$ cm^3; the long-dashed curve corresponds to the maximum s-wave capture rate coefficients with $P_s(\kappa) = 1$).

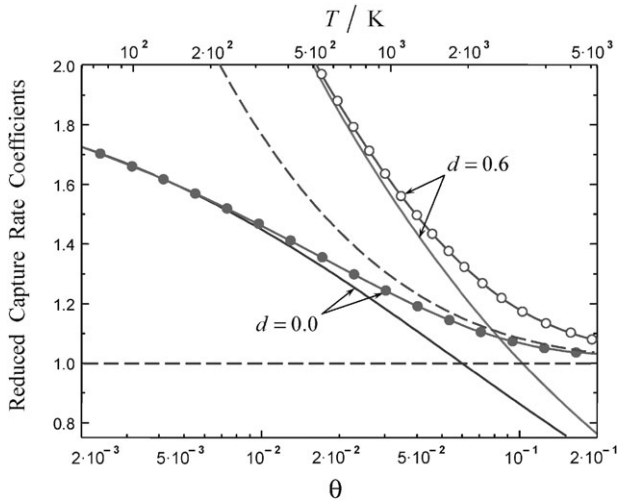

Fig. 6 Comparison of reduced quantum all-wave (lines with circles) with quantum s-wave capture rate coefficients (full lines); dashed lines are classical capture rate coefficients, the upper temperature scale is as in Fig. 5.

4. All-wave electron capture by polar plus polarizable target molecules

The analysis of the second-order perturbation calculation of D_{jm} for the range $0 < d < 1$ shows that the eigenvalues D_{jm} for higher partial waves cluster around the respective values for the dipoleless capture, *i.e.* around $\ell(\ell + 1)$. For values of d which are of interest for electron–molecule collisions, this clustering virtually does not show up in the higher partial wave contributions to the capture rate coefficient. One can therefore provide an approximation to this contribution by identifying it with the respective contribution for the capture by a dipoleless molecule. This argument leads to the following all-wave analytical expression for the capture rate coefficient

$$\chi_{all}(\theta, d) \approx \chi_{all}(\theta) + \left[\chi_s^{max}(\theta) - \chi_s(\theta)\right] \times \{1 - \exp[-G(\theta, d)]\} \quad (4.1)$$

where $\chi_s(\theta, d)$, $\chi_s(\theta)$, $\chi_{all}(\theta)$ are given by eqns (3.9), (2.14) and (2.15), respectively. Plots of $\chi_{all}(\theta,d)$ for $d = 0$ and for $d = 0.6$ are shown in Fig. 6 together with the partial contributions $\chi_s(\theta, d)$. At this point, one should compare the all-wave quantum rate coefficients with their classical counterparts. The reason for such a comparison follows from the observation that the higher partial wave contributions to the capture rate coefficient are satisfactorily described by classical approximation[4] and that quantum effects in the probability for s-wave capture, which cause it to be smaller than unity, are not very large, see Fig. 4. In previous classical trajectory calculations,[14,15] extending the work by Su and Chesnavich,[16] we have systematically analyzed the full dynamics of capture between the adiabatic (Massey parameter $\gg 1$) and the sudden (Massey parameter $\ll 1$) limits. For the sudden limit, the results of ref. 14 and 15 can be written in the form

$$\chi_{all}^{cl} = k_{cap}^{cl}/k_L = (2d^2/\pi^2\theta)^{1/4} F(\theta) \quad (4.2)$$

with

$$\ln F(\theta) = a_0 + (a_1^2 z/\sinh z + z^2/16)^{1/2} \quad (4.3)$$

where $z = a_2 + \ln(\theta\, 2d^2)$, $a_0 = -0.407$, $a_1 = 0.425$, and $a_2 = 3.921$. The limits for a dominating permanent dipole ($2\theta/d^2 \ll 1$) and dominating polarizability ($2\theta/d^2 \gg 1$) are $\chi_{all}^{cl} \Rightarrow (8\pi\theta/d^2)^{-1/2}$ and $\chi_{all}^{cl} \Rightarrow 1$, respectively.

The comparison between quantum and classical rate coefficients is illustrated in Fig. 6. The case $d = 0$ was discussed in detail in ref. 4. In short, the low-temperature overshoot of the quantum rates beyond the classical rates reflects the fact that the zero-temperature Bethe–Wigner s-wave rate is twice the Langevin rate. For $d = 0.6$, the comparison of the quantum and classical rates reflects the interplay of two types of interaction, charge–permanent dipole and charge–induced dipole. In the limit of very low temperatures when the latter prevails, the classical rate given by $\chi_{all}^{cl}(\theta, d) = (d/2)/\sqrt{2\pi\theta}$ is higher than its s-wave quantum counterpart, $\chi_{all}^{cl}(\theta, d) > \chi_s(\theta, d)$. This is evident from eqn (3.8) and the plots in Fig. 5 where the slopes of the curves are smaller than the slope of the curve that corresponds to $\chi_s^{max}(\theta) = 1/\sqrt{2\pi\theta}$. However, the relation $\chi_{all}^{cl}(\theta, d) > \chi_s(\theta, d)$, valid for very low temperatures, is inverted within the temperature range of Fig. 6, implying that $\chi_{all}^{cl}(\theta, d) < \chi_s(\theta, d)$. One of the reasons for this inequality is that for the temperatures $10^{-3} < \theta < 10^{-1}$ and dipole moments in the range $0 < d < 1$, the contribution of the charge–induced dipole interaction is substantial and cannot be neglected. Finally, we emphasize that the given results are only valid when only one of the capture channels is open classically, that is when all D_{jm} with $jm \neq s$ are positive and not too small. For instance, the smallest positive eigenvalue D_{jm} of about unity occurs for $d \approx 3$.

Table 1 Rate coefficients for electron attachment at 300 K (k_{at}, experimental) and for s-wave electron capture ($k^a_{cap,s}$: calculated with polarizability only, $k^b_{cap,s}$: calculated with polarizability and dipole moment, references in parentheses)

Molecule	k_{at}/cm^3 s^{-1}	$\alpha/10^{-24}$ cm^3	μ_D/D	$k^a_{cap,s}$/cm^3 s^{-1}	$k^b_{cap,s}$/cm^3 s^{-1}
SF_6	2.25×10^{-7} (7)	6.54 (19)	0.0	2.81×10^{-7}	2.81×10^{-7}
CCl_4	3.6×10^{-7} (22)	11 (19)	0.0	3.18×10^{-7}	3.18×10^{-7}
SF_5Cl	4.8×10^{-8} (25)	9.5 (25)	0.54 (25)	3.07×10^{-7}	3.15×10^{-7}
$POCl_3$	5.1×10^{-8} (26)	13.2 (26)	1.2 (26)	3.30×10^{-7}	3.73×10^{-7}
CHF_3	$\sim 4 \times 10^{-14}$ (27)	3.55 (19)	1.65 (19)	2.36×10^{-7}	3.53×10^{-7}
CH_2Br_2	9.6×10^{-8} (22,28)	9.32 (19)	1.43 (19)	3.06×10^{-7}	3.75×10^{-7}
$CFCl_3$	2.38×10^{-7} (29,30)	9.47 (20)	0.46 (19)	3.07×10^{-7}	3.31×10^{-7}

5. Practical examples for capture rate coefficients

There are numerous experimental determinations of thermal electron–molecule attachment rate coefficients, see *e.g.* the reviews by Smith and Španěl[17] and Miller.[18] We cannot possibly compare all of these results with calculations of capture rate coefficients employing the present relationships. We can select a few representative examples only, emphasizing however that the calculation is straightforward when polarizabilities[19,20] α and dipole moments[19,21] μ_D are known. Table 1 illustrates the results. One can notice that in some cases, like electron attachment to SF_6 and CCl_4, the attachment rate coefficients reach up to the s-wave capture rate coefficients calculated in the present article which should provide upper limits of the attachment process (as long as higher partial-waves do not contribute). In other cases, like electron attachment to CHF_3, they fall far below. A quantitative rationalization of this phenomenon appears highly desirable but cannot be the subject of the present article, see ref. 6. One can also notice that the contributions due to the permanent dipole moments are rather small. We have also estimated contributions due to quadrupole moments and found that these can practically always be neglected. In practice, the present approach will be helpful when conflicting values of attachment rate coefficients are derived by different methods, *e.g.*, discharge flow studies of dissociative electron attachment to CCl_4 from ref. 22 led to the value given in Table 1 in close agreement with the Vogt–Wannier attachment rate coefficient. On the other hand, laser photoelectron attachment[23] and Rydberg electron transfer[24] data gave about 4 times larger values, which was tentatively attributed to the participation of bound anion states. The present calculations rather suggest that the latter data require a recalibration of the absolute values of the rate coefficients.

6. Conclusions

The present article, in the spirit of the Vogt–Wannier model[2] and its extension by Fabrikant and Hotop,[1,3] has provided analytical approximations for cross sections and thermal rate coefficients for capture of electrons by polarizable and dipolar target molecules. The treatment illustrates the relation between electron and atom (or molecule, neutral or charged) capture by dipolar molecules such as treated in ref. 4. In addition, the relation of the sudden capture dynamics for electrons and often nearly adiabatic capture dynamics for heavier particles can be recognized. Comparing experimental rate coefficients for electron attachment with the capture rate coefficients calculated here, one notices that the latter provide an upper bound to the former and may be understood as electron–molecule "collision numbers". The differences between calculated capture and measured attachment rate coefficients call for more systematic investigations, relating the differences to the individual molecular properties of the target species and, by this, identifying the competing processes which follow the initial capture event. Such an investigation is underway in our group.[6]

Appendix. Electron capture by polarizable molecules

Analytical representation of the capture probabilities for $\ell \geq 1$

$$P_l(\kappa) = (2\kappa/\kappa_c)^{2l+1} G_l(\kappa_c/2) \quad \text{for} \quad \kappa \leq \kappa_c/2$$

$$P_l(\kappa) = G_l(\kappa) \quad \text{for} \quad \kappa \geq \kappa_c/2$$

$$G_l(\kappa) = 0.5 + 0.5[1 + \tanh H_l(\kappa)]$$

$$H_l(\kappa) = a_l(\kappa - \kappa_c) + b_l(\kappa - \kappa_c)^2 + c_l(\kappa - \kappa_c)^3$$

Here the parameters κ_c, a_l, b_l, and c_l given by:

ℓ	κ_c	a_l	b_l	c_l
1	1.18	1.50	−0.50	0.10
2	3.20	0.90	−0.15	0.02
3	6.15	0.65	−0.06	0.004
4	10.2	0.47	−0.02	0.003

A graphical representation of $P_l(\kappa)$ is given in Fig. 1 of ref. 4 and the present analytical representations are indistinguishable from the figure.

Acknowledgements

Many helpful discussions of this work with T. M. Miller and A. A. Viggiano are gratefully acknowledged.

References

1 H. Hotop, M.-W. Ruf, M. Allan and I. I. Fabrikant, *Adv. At. Mol. Opt. Phys.*, 2003, **49**, 85.
2 E. Vogt and G. H. Wannier, *Phys. Rev.*, 1954, **95**, 1190.
3 I. I. Fabrikant and H. Hotop, *Phys. Rev. A: At., Mol., Opt. Phys.*, 2001, **63**, 022706.
4 E. E. Dashevskaya, I. Litvin, A. I. Maergoiz, E. E. Nikitin and J. Troe, *J. Chem. Phys.*, 2003, **118**, 7313.

5 C. E. Klots, *Chem. Phys. Lett*., 1976, **38**, 61, see also M. Quack and J. Troe, *Ber. Bunsen-Ges. Phys. Chem*., 1974, **78**, 240.
6 J. Troe, T. M. Miller and A. A. Viggiano, in preparation.
7 J. Troe, T. M. Miller and A. A. Viggiano, *J. Chem. Phys*., 2007, in press.
8 J. Troe, T. M. Miller and A. A. Viggiano, *J. Chem. Phys*., 2007, in press.
9 J. E. Wollrab, *Rotational Spectra and Molecular Spectra*, Academic Press, New York and London, 1967.
10 K. Takayanagi, *J. Phys. Soc. Jpn*., 1978, **45**, 976.
11 A. I. Maergoiz and J. Troe, *J. Chem. Phys*., 1993, **99**, 3218.
12 A. I. Maergoiz, J. Troe and Ch. Weiss, *J. Chem. Phys*., 1994, **101**, 1885.
13 J. Troe, *J. Chem. Phys*., 1987, **87**, 2773.
14 A. I. Maergoiz, E. E. Nikitin, J. Troe and V. G. Ushakov, *J. Chem. Phys*., 1996, **115**, 6263.
15 E. I. Dashevskaya, A. I. Maergoiz and V. G. Ushakov, *Z. Phys. Chem*., 2002, **216**, 605.
16 T. Su and W. J. Chesnavich, *J. Chem. Phys*., 1982, **76**, 5183.
17 D. Smith and P. Španěl, *Adv. At. Mol. Opt. Phys*., 1994, **32**, 307.
18 T. M. Miller, *Adv. At. Mol. Opt. Phys*., 2005, **51**, 299.
19 *Handbook of Chemistry and Physics*, ed. D. R. Lide, CRC Press, Boca Raton, 85 edn, 2004.
20 H. Kagawa, A. Ichimura, N. A. Kamka and K. Mori, *THEOCHEM*, 2001, **546**, 127.
21 A. L. McClellan, *Tables of Experimental Dipole Moments*, Freeman, San Francisco, 1963.
22 S. J. Burns, J. M. Matthews and D. L. Mc Fadden, *J. Phys. Chem*., 1996, **100**, 19436.
23 D. Klar, M.-W. Ruf and H. Hotop, *Int. J. Mass Spectrom*., 2001, **205**, 93.
24 M. T. Frey, S. B. Hill, K. A. Smith, F. B. Dunning and I. I. Fabrikant, *Phys. Rev. Lett*., 1995, **75**, 810.
25 J. M. Van Doren, T. M. Miller, A. A. Viggiano, P. Španěl, D. Smith, J. Bopp and J. Troe, *J. Chem. Phys*., 2008, in press.
26 W. B. Knighton, T. M. Miller, E. P. Grimsrud and A. A. Viggiano, *J. Chem. Phys*., 2004, **120**, 211.
27 L. G. Christophorou and J. K. Olthoff, *Fundamental Electron Interactions with Plasma Processing Gases*, Kluver/Plenum, New York, 2004.
28 A. Schramm, M.-W. Ruf, M. S. Tano, S. Matejcik, I. I. Fabrikant and H. Hotop, *J. Phys. B*, 2002, **35**, 4179.
29 D. Klar, M.-W. Ruf, I. I. Fabrikant and H. Hotop, *J. Phys. B*, 2001, **34**, 3855.
30 O. J. Orient, A. Chutjian, R. W. Crompton and B. Cheung, *Phys. Rev. A: At., Mol., Opt. Phys*., 1989, **39**, 4494.

